UV-A photocatalytic treatment of *Legionella pneumophila* bacteria contaminated airflows through three-dimensional solid foam structured photocatalytic reactors

Sébastien Josset [a], Shabnam Hajiesmaili [a], Dominique Begin [a], David Edouard [a], Cuong Pham-Huu [a], Marie-Claire Lett [b], Nicolas Keller [a,*], Valérie Keller [a]

[a] *Laboratoire des Matériaux, Surfaces et Procédés pour la Catalyse (LMSPC), European Laboratory for Catalysis and Surface Sciences (ELCASS), CNRS, Strasbourg University, 25 rue Becquerel 67087 Strasbourg, France*
[b] *Laboratoire de Génétique Moléculaire, Génomique, Microbiologie, CNRS, Strasbourg University, 28, rue Goethe 67083 Strasbourg Cedex, France*

ARTICLE INFO

ABSTRACT

A 3D-structured photocatalytic media was designed for allowing a tubular reactor to work in a traversing-flow mode at low pressure drops with a strong increase in the surface area-to-volume ratio inside the reactor. A protective polysiloxane coating was performed for protecting a structured polyurethane foam and anchoring the active TiO_2 particles. Filled with the 3D-structured solid foam supporting TiO_2 photocatalyst, the reactor could thus take advantages from the static mixer effect and from the low pressure drop resulting from the reticulated foam support. Very efficient decontamination levels towards airborne *Legionella pneumophila* bacteria were reached in a single-pass test mode.

© 2009 Elsevier B.V. All rights reserved.

1. Introduction

Recently, De Lasa et al. have stated, "there is general agreement that an important obstacle in the development of highly efficient photocatalytic reactors is the establishment of effective reactor designs for intermediate and large-scale use, as demanded by industrial and commercial applications" [1]. They claimed that achieving a successful commercial implementation will require the optimization of several reactor design parameters, such as the photoreactor geometry, the type of photocatalyst and the utilization of radiated energy.

The slurry reactor is actually an efficient and widespread reactor configuration, although it strongly suffers notably from the need of restrictive filtration processes for recovering the photocatalyst particles. This drawback could be overcome by the development of immobilized TiO_2 photoreactors, the photocatalyst being coated on the reactor walls surrounding the light source or anchored to a solid supports such as listed by De Lasa et al. [1]. In this configuration, immobilized catalyst photoreactors allow a continuous use of the photocatalyst, although they actually suffer from drawbacks like a low surface area-to-volume ratio, a low light utilization efficiency, non-negligible pressure drops, catalyst fouling or wash out, and possible mass transfer limitations [2].

The removal of airborne chemical or biological pollutants is a promising field of applications for photocatalysis, and the treatment of relatively large gas flows with low pressure drops together with a good photocatalyst irradiation and an efficient photocatalyst/reactant contact remains challenging [3]. Novel designs of photocatalytic reactors are thus expected to be engineered for overcoming restrictive efficiency limitations and meeting the performance requirements for achieving a successful commercial implementation.

Among several strategies, many photocatalytic reactor configurations and designs have been developed for air applications [1,3–6]. The annular geometry remains interesting for controlling volatile organic compound (VOC) emissions in indoor air, since it benefits from a maximal direct and radial irradiation issued from the lamp located inside the inner central tube of the reactor. However, this annular reactor configuration suffers from a low area of photocatalyst per unit reactor volume, which is strongly restrictive in terms of gas velocity. In parallel, the need for a good contact between the air and the photocatalyst when processing high flows at a low pressure drop has put forward the use of porous or multichannel materials, among which honeycomb-shaped monoliths were investigated from both modelling and experimental aspects

[7–10]. However, the monolith-based materials also suffer from poor irradiation distribution, although progress can be made by optimizing the distribution of irradiation in such reactors [11].

Recently, Zahraa and co-workers studied the influence of the geometry of a monolith support on the efficiency of photocatalysts for air cleaning, by designing Nd-YAG laser assisted stereolithography-shaped epoxy resins as 3D supports for TiO$_2$ layers, and further by investigating the static mixer, the crossed channels and the star geometry configurations using methanol as model VOC [12]. They developed a model that described the basic phenomena involved, such as light absorption, hydrodynamic and transfer processes and also reaction kinetics.

Following the pioneering work of Lin and Valsaraj [13] on wastewater treatment, Moulijn and co-workers have combined both honeycomb-shaped monolith and optical fiber approaches, with "side light fibers" evenly distributed inside a ceramic monolith structure, on the inner walls of which a TiO$_2$ photocatalyst was coated [14]. This geometry was interesting for taking advantages from the remote delivery of photon to the reactive sites of the photocatalysts.

Recently solid foam structures received more and more interest as catalytic support in order to overcome some of the drawbacks of 'conventional' packed beds. This attractive medium in the catalysis field has a highly permeable porous structure with high porosity (0.60–0.95), which enables a considerable reduction of the pressure drop along the catalyst bed even at high space velocity, together with a high effectiveness in mass transfer properties [15,16].

Jain and Pradeep used the bactericidal properties of silver nanoparticles anchored on a polyurethane foam for obtaining a logarithmic abatement of 5 over *Escherichia coli* contaminated water at a water flow rate of 0.5 L/min and a residence time close to 1 s [17]. The silver nanoparticles were uniformly coated on the foam with possible interactions with the nitrogen atoms of the polyurethane. The authors claimed that the coated foam can be used as a low cost drinking water filter in developing countries where bacterial contamination of the surface water is a health risk.

Yamamoto and Imai prepared foam-based photocatalysts, with the synthesis of anatase titania nanoparticle foams with open cellular structure by calcination of polyacrylamide gels containing titanyl sulfate and urea [18]. The titania foams showed under UV-A illumination a disappearance rate 2.5 and 4 times greater than that shown by fluffy commercial TiO$_2$ P25 in the case of methylblue dye decomposition in water and gas phase acetaldehyde removal, respectively. The performances were attributed to the high accessibility and the high transparency of UV light due to an open cellular structure with wide channels and thin walls. Using the photocatalytic oxidation of 1,8-diazabicyclo[5.4.0]undec-7-ene in water, Ochuma et al. evidenced the interesting performances of a TiO$_2$-coated alumina reticulated foam monolith inserted inside an annular photoreactor, compared to a slurry reactor [19].

Crossing-over between photocatalysis and life science is a growing research area, since Matsunaga et al. opened the door by reporting on the microbiocidal effects of TiO$_2$ in water [20]. This gave rise to extensive research in the field of the biological applications of TiO$_2$ photocatalysis, mainly dealing with self-decontaminating surfaces, or water disinfection using TiO$_2$ suspensions [21–24]. In contrary to surface and liquid phase applications, works on the photocatalytic disinfection of contaminated air by pure UV-A photocatalysis remained scarce, mainly targeting *E. coli* and *Legionella pneumophila* bacteria, *Bacillus atrophaeus* endospores, MS2 and λ phage viruses, despite the great interest for public health reasons and a large spectrum of applications [25–29]. This resulted probably from the difficulty in generating reproducible airborne microorganism contaminated airflows, from the representative airflow sampling, and from the setting of specific biological numeration techniques.

Here, regarding the need for low pressure drop and high contact surface photoreactors, we report on the use of reticulated alveolar polyurethane foam as 3D-structured photocatalytic support. UV-A photocatalysis was used for the efficient *on-stream* treatment of airborne *L. pneumophila* bacteria at a 5 m^3/h airflow, this bacteria being used as model biological target and remaining also a problematic microorganism responsible for the legionnaire's disease and the Pontiac fever. The photocatalytic material was characterized and its impact on the decontamination efficiency of a tubular photoreactor was pointed out.

2. Experimental

2.1. Material preparation

2.1.1. The polyurethane foams

The foam can be manufactured with different geometries and shapes, allowing for example the adjustment of axial or radial flow patterns in the reactor. The pore structure of typical commercial foams, shown in Fig. 1, evidenced a high degree of interconnectivity through the entire matrix of the foams. The small thickness of the struts constituting the solid foams is beneficial to mass transfer properties. Most characteristic parameters are the size of the cell (Φ), the windows (or pore diameter (a)), which can be measured by several techniques and correlated with the pore density (the number of pores per linear inch, ppi) and the struts diameter (ds).

2.1.2. Protection of the PU foam and TiO$_2$ deposition

Dynasylan® SIVO 110 (Evonik) is a monodispersed silica sol modified with organofunctional silanes. Due to a high concentration of active silanol functions, it can chemically bond to surfaces of suited materials (such as TiO$_2$ in the present study) and achieves a high degree of crosslinking by formation of 2D and 3D siloxane networks. During curing, functionalized SiO$_2$ sol-particles align into a dense packed structure and are covalently incorporated into the siloxane network for providing hardness and scratch resistance to the formed composite. The formation of the polysiloxane protective film occurred through condensation steps between Y-(CH$_2$)$_n$-Si(OH)$_3$ molecules and by reacting further with hydroxyl surface groups of TiO$_2$ particles. The organic function of this bifunctional organosilanetriol molecule, *i.e.* the Si-bonded epoxy groups, is responsible for the grafting of the film onto the organic surface of the PU.

The protection of the PU foam rings was performed following a three step procedure. The rings were first immersed in a SIVO110 solution at 50% (v/v) in ethanol. Opening of alveolus that could be possibly closed by the film was then achieved under pressurized air for a few seconds, before the final polymerization step at 120 °C for 15 min in air was performed. This sequence was triplicated. A final immersion of the protected PU foam into the SIVO110 ethanol solution was performed, but without any polymerization treatment, so that a viscous film remained at the PU ring surface, available for anchoring the TiO$_2$ powder after the evaporation of the ethanol solvent at room temperature. A final polymerization step at 150 °C for 30 min in air was performed for allowing the chemical bonding between the photocatalyst and the protected PU foam to be achieved.

2.2. Characterization techniques

Scanning Electron Microscopy (SEM) was carried out on a JSM6700F JEOL microscope.

Experimental pressure drop was measured using the apparatus described in Ref. [30], equipped with a 0–200 mbar differential pressure sensor, on 0.1 m long materials varying the gas velocity in the 0–8 m/s range.
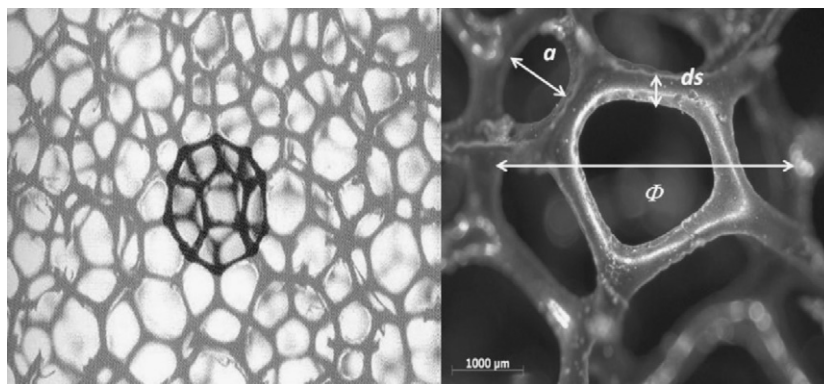
Fig. 1. Polyurethane foam images, evidencing the cell size (Φ), the window size (a) and the strut diameter (ds) characteristics.

The light transmission through the structured media was measured by comparing the (I_0) intensity of the UV-A lamp at the maximum intensity wavelength to that of the transmitted light after passing through the foam (I_t), using a RPS900 SpectrILight radiometer. The I_t/I_0 behavior was obtained by changing the thickness t of the foam.

Quantitative analysis was achieved by epifluorescence microscopy using the "LIVE/DEAD Baclight Bacterial Viability kit®" (Invitrogen®) as appropriate viability indicator and staining method based on a membrane integrity test. This double staining method is based on two stains, propidium iodide (PI) and SYTO9™, which differ in their ability to penetrate bacterial cells [31]. Based on the fluorescent properties of dyes bound to specific cell components, fluorescence methods are considered as the easiest way to count the number of viable bacteria, and provide a direct count since they rely on the direct observation of the cells and allow targeting of very specific characteristics of the state or of the metabolic activity of a microorganism.

This numeration procedure is based on the non-selectivity of the SYTO9™ stain towards the integrity of cell membranes: SYTO9™ penetrates the cell membrane whatever its integrity (integrate as well as damaged membranes), whereas PI only enters the damaged cells. With integrate membranes, the SYTO9™–DNA complex lets the living cells fluoresce green, while the higher affinity of PI to DNA removes the SYTO9™–DNA complex when both dyes are present, and PI reacts with the DNA, which lets the dead cells emit red light. As a consequence, when used alone, SYTO9™ stain labels both living and dead bacteria, while in contrast, PI stain labels only bacteria with damaged membranes. More details can be found in a recent review [31].

2.3. Experimental device, procedure and protocols

The micropilot used for the *single-pass* UV-A photocatalytic treatment of contaminated air, located inside a safety glove box adapted for airborne bacteria manipulations, both previously described [27] and schematized in Figure S1, Supporting Information. It consists of an air inlet line composed of glass vessels and filters for purifying the air introduced from a compressor, from oil residue, dust particles, gaseous pollutants and contamination by external microorganisms. Sterilization was achieved using a Kleen-pack filter with Emflon® PFR Membrane Assemblies (Pall) with a cut-off of 0.003 μm. A glass vessel was filled with activated charcoal for removing gaseous contaminants. An aqueous suspension of *L. pneumophila* bacteria was aerosolized in the inlet airflow at a controlled injection rate using a peristaltic pump. The contaminated air flow subsequently passed through the *single-pass* photocatalytic reactor, and the bacteria in the effluent stream were further collected *on-line* downstream of the photoreactor in a glass bubble column containing sterile water. To prevent any release of bacteria out of the glove box, another Kleenpack filter was placed downstream of the column, before the final outlet flow evacuation.

Due to their low bacteria concentration, the collected suspensions (50 mL) were first concentrated, by filtering them on a 25 mm diameter and 0.4 μm porosity black polycarbonate Isopore Filter Membrane (Millipore). The bacteria-loaded filter was then deposited on the microscope slide, and further impregnated with a SYTO9 or PI aqueous solution (160 μL). Extensive details can be found in Ref. [31]. Whatever the dye, the staining was performed for 15–20 min.

The reactor consisted of a 26 cm length and 7 cm diameter stainless steel tubular reactor, with a 1.8 cm diameter commercial 8W UV-A black-light (spectral peak centred at 365 nm, BLB F8 T5 model from Philips) axially maintained at the centre of the reactor. In the case of the tubular reactor working in the seep-flow mode, the TiO₂ coating was performed by evaporating to dryness aqueous slurry of the TiO₂ and the coated reactor was further dried at 110 °C for 1 h in air. Fig. 2 shows a schematic view of the tubular reactor working in the seep-flow mode, and of the tubular photoreactor filled with the 3D-structured reticulated solid foam for working in a traversing-flow mode (with a 2.5 cm foam thickness).
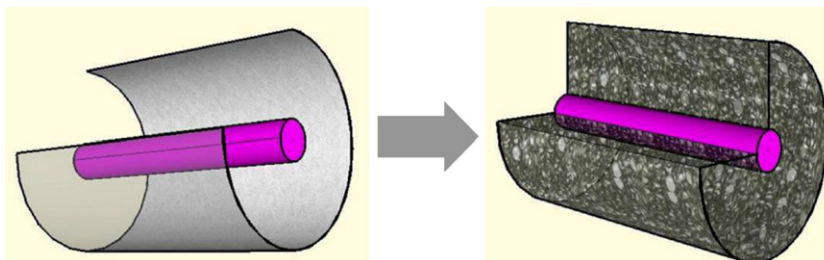

Fig. 2. Schematic view of the tubular photoreactor (*left*) without and (*right*) with the 3D-structured foam.

L. pneumophila (strain GS3.11) was grown within 24 h at 37 °C on agar plates (Buffered Charcoal Yeast Extract Medium, BCYE, Biomérieux), from a −80 °C stored strain sample. About 10 glass beads and 2 mL of distilled water were added to each plate under sterile conditions before vigorous shaking in order to recover the beads with the bacteria. The concentrated solution was further diluted for obtaining a total volume of 40 mL. Finally, few glass beads were added to the suspension for performing a brief shaking in order to disaggregate bacterial packs.

2.4. Logarithmic reduction in viability and bacteria survival probability

The decimal logarithmic abatement or logarithmic reduction (LR) was considered as the efficiency indicator associated to a liquid or surface disinfection process for expressing results in microbiology, rather than the percents as when working with chemicals. This indicator compared the concentrations before and after the treatment, so that the treatment efficiency was defined by this ratio, expressed in magnitude order for overcoming the low precision of biological numerations [31]. However, this way of calculation was only representative if the totality of the microorganisms could be numerated, and in the present study, the numeration could unfortunately not be performed over the totality of the bacteria. Therefore, the fluorophore-based epifluorescence microscopy was preferred as powerful technique for numerating both live and dead bacteria. The viability of bacteria in the inlet and the outlet streams, defined as the ratio between the live bacteria and both live and dead bacteria in the air sampling was thus to consider. The viability of the bacteria in the inlet air corresponded to the viability of the starting suspension (μ_i), whereas the viability of the bacteria in the outlet air corresponded to the viability of the collected suspension (μ_o). It should be noted that the absence of any influence of both aerosolization and collection processes on the bacteria viability has been checked. As a result, the logarithmic reduction has been replaced by the logarithmic reduction in viability (LRV) expressed as follows:

$$\mathrm{LRV} = \log \frac{\mu_i}{\mu_o}$$

with μ_i and μ_o being the viability of bacteria in the inlet and outlet stream, respectively.

In addition, the probability P_v for a bacteria to come out of the reactor alive was given by $P_v = 10^{-\mathrm{LRV}}$.

Considering that the experimental probability P_v corresponded to the survival probability for a reactor of length $L_r = 26$ cm, *i.e.* $P_v = P(L_r = 26)$, and assuming the first hypothesis of a first order kinetic and a of Plug Flow Reactor mode, the survival probability per unit of reactor length could be defined as $P(1) = P(L)^{1/L}$. The survival probability of a bacteria as a function of the reactor length (L) could thus be given by $P(L) = P(1)^L$. In a first assumption, this probability was interesting for roughly extrapolating the decontamination efficiency of the photocatalytic reactors as a function of the reactor length. The illumination power corresponding to a reactor length of L should be extrapolated to $8xL/26$ W to provide a constant illumination whatever the reactor length.

3. Characterization of the 3D-structured alveolar foam materials

3.1. Morphological parameters

Several researchers have developed relations between the macroscopic structural parameters of the solid foams such as the strut diameter, the pore size and the relative foam density (or porosity), available in routine measurements, and no general con-

sensus was observed up to now due to the complexity of the geometric shape of these porous medium. These cells could be modelled for example by a polyhedra [32], tetrakaidecahedron [15,33], or cubic form [34].

Fig. 3A shows the SEM image of the PU foam surface passivated by the polysiloxane protective coating, evidencing the homogeneous and smooth surface coverage, although some inevitable cracks could be observed at the sample surface. After the homogeneous deposition of TiO$_2$ particles, evidenced by Fig. 3B, the
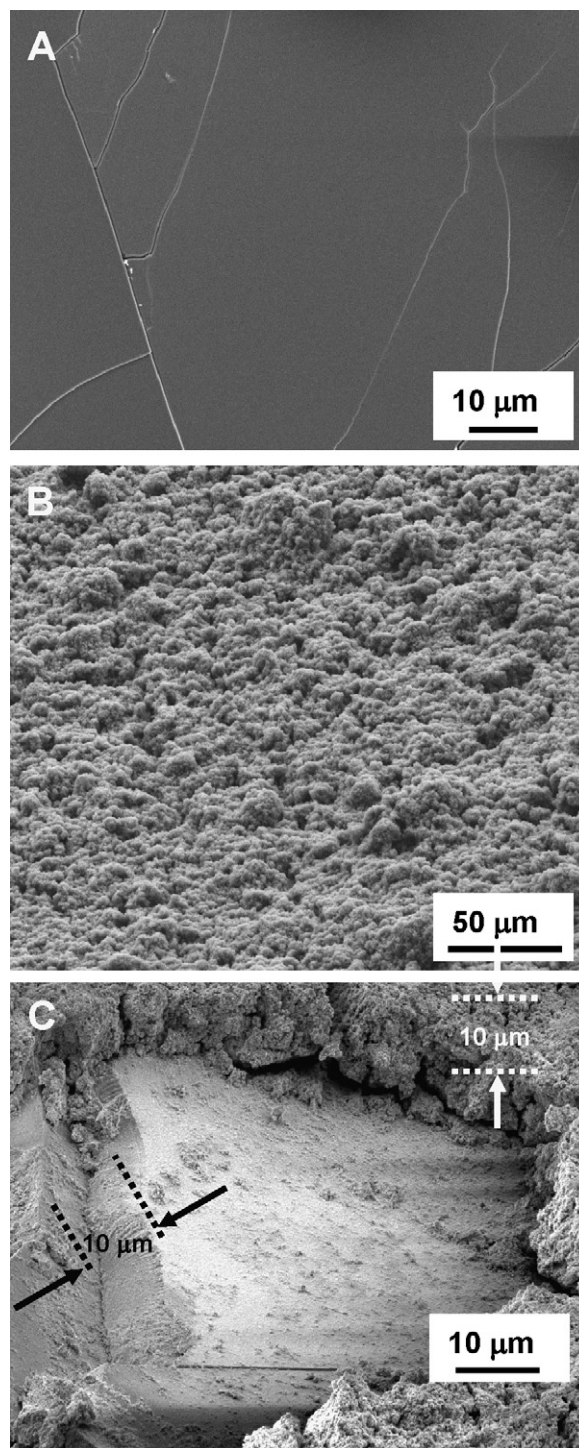

Fig. 3. SEM images of (A) the PU foam surface passivated by the polysiloxane coating, (B) the homogeneous TiO$_2$ coating and (C) a scratched zone evidencing the thickness of both polysiloxane and TiO$_2$ coatings on the PU surface.

smooth aspect of the surface of the protected polyurethane foam was changed into the rough aspect shown by the surface of the TiO_2 particle coating. This rough nature could be of high interest for better impacting the micrometer-size bacteria compared to a smooth surface. A scratched zone of the sample shown in Fig. 6C allowed the mean thickness of the TiO_2 coating and of the polysiloxane layer being evaluated at 10 μm.

3.2. Geometrical surface area and open porosity

One of the interests of using the 3D-structured alveolar foam is the high gain in surface exposed to the reaction flow per unit reactor volume, and thus the increase in the surface area-to-reactor volume ratio, compared to a tubular photocatalytic reactor with a thin inner layer of TiO_2. The gain in surface available for performing photocatalysis was therefore an important parameter to evaluate.

The specific surface area of the solid foams could be determined as a function of the porosity, the pore diameter or the strut diameter. The main difference reported in literature was due to the different geometrical models used for describing the solid foam matrix. Independently of the pore size, the evolution of the specific surface area as a function of the solid foam porosity showed very close results with different models developed by Lacroix et al. [30], Fourie and Du Plessis [32] and Buciuman and Kraushaar-Czarnetzki [33]. All the models exhibited a linear relationship with the pore diameter.

Only few authors compare the estimated specific surface area with the experimental data. Tadrist et al. [34] and Moreira and Coury [35] measured the specific surface area in m^{-1} by image analysis. The authors have considered the perimeters of the solid phase of a cross-section of the foam and multiplied it by the length. In this context, the following paragraph describes a method for evaluat-
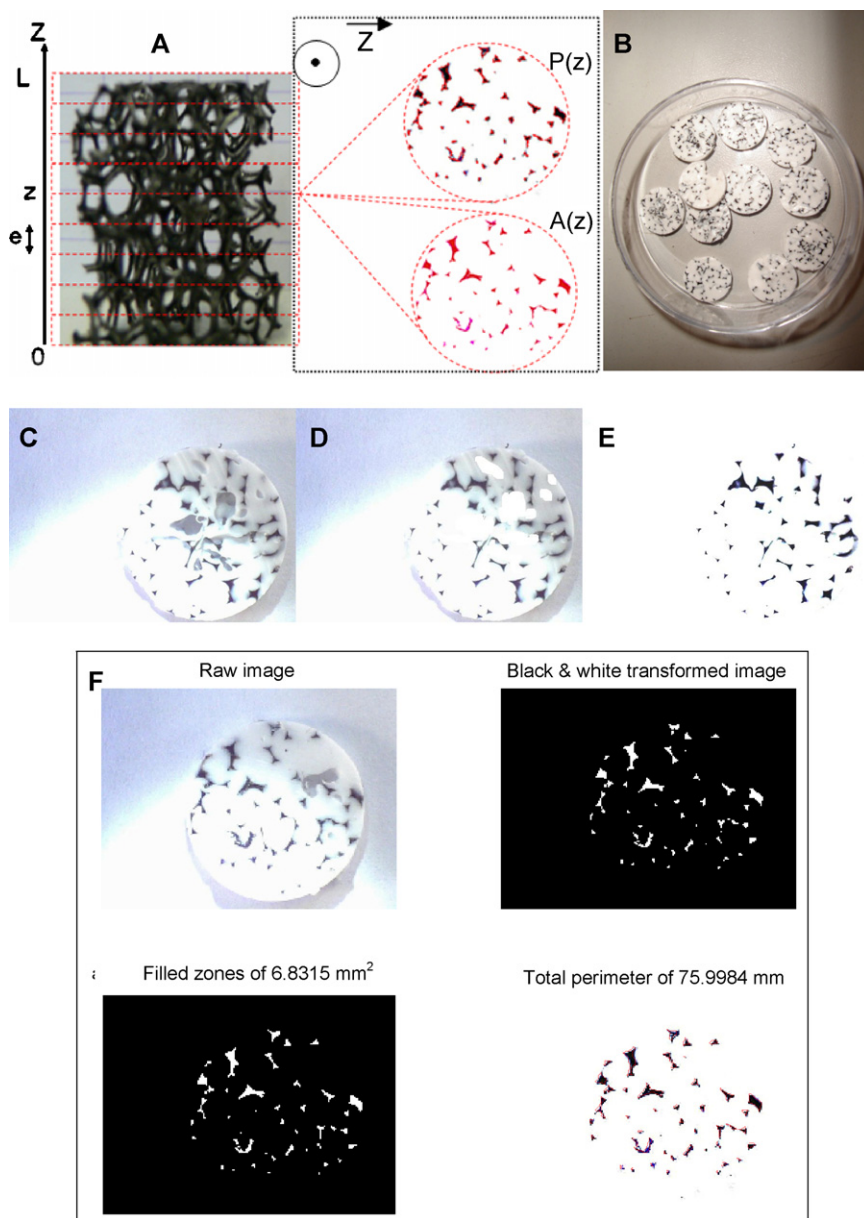

Fig. 4. (A) PU foam roll with its *Z*-coordinate and top-view of the cross-section slice at *Z* = *z* (the intersection perimeters and surfaces are reported in red). (B) PU foam–silicone mixed slices. (C) Raw image of a PU foam–silicone mixed slice. (D) Image of a PU foam–silicone mixed slice after bubble filling. (E) Image of a PU foam–silicone mixed slice after increasing the contrast. (F) Treatment of the PU foam cross-section slices using Matlab®; (*top left*) raw image of a PU foam cross-section slice; (*top right*) Image with filled bubbles, black&white reverse treatment and maximized contrast; (*bottom left*) image after removal of "isolated" pixels (*i.e.* only with filled surface); (*bottom right*) outline determination and perimeter measurement). (For interpretation of the references to color in this figure legend, the reader is referred to the web version of the article.)

ing the gain in surface provided by the filling of the reactor by the 3D-structured alveolar foam compared to a hollow tubular photoreactor with TiO_2 covering the inner surface of the reactor wall. Following that, the foam roll was discretized into slices of thickness dz and the geometrical surface developed by each elemental slice was derived. In parallel, the foam porosity could also be derived, by calculating the intrinsic volume of matter in each elemental slice.

Regarding a PU foam cylinder of height L, each z X-coordinate led to ascribe $P(z)$ and $A(z)$ as the total perimeter and the total surface, of the intersections of the PU foam with the plane expressed as $Z = z$, respectively (Fig. 4A). The geometrical surface S and the volume V of the PU foam could be rigorously defined as

$$S = \int_0^L P(z)dz \quad V = \int_0^L A(z)dz$$

Then, they could be expressed as

$$S = L \left(\frac{1}{L} \int_0^L P(z)dz \right) = L \times P_r \quad V = L \left(\frac{1}{L} \int_0^L A(z)dz \right) = L \times A_r$$

with P_r and A_r, being respectively the mean real values of the perimeter and of the surface of the intersection of the $Z = z$ plane with the PU foam contained inside the control cylinder for z ranging from 0 to L. Assuming a division of the control cylinder into n equally-thick slices, both expressions could be represented as

$$P_r = \lim_{n \to \infty} \frac{1}{n} \sum_{k=0}^{n} P \left(k \frac{L}{n} \right) \quad A_r = \lim_{n \to \infty} \frac{1}{n} \sum_{k=0}^{n} A \left(k \frac{L}{n} \right)$$

As a result, the measurement of the surface and of the perimeter of N control cylinder slices (N being a finite number) led to estimate P_r and A_r, and thus both surface and volume of the PU foam per volume unit. Bigger N, more precise the estimation.

Experimentally, a PU foam roll (18 mm diameter and 20 mm height, foam with cell size $\geq 4800 \mu m$) was used. Silicone oil-fluidized white silicone was further injected through a syringe inside the roll, maintained inside a plastic rigid scroll. After a two week polymerization, the resulting inclusion was slowly pushed out of the tube and further sliced using a razor blade into 1 mm thick slices (Fig. 4B). Images of the different slices were then taken using an optical microscope (Fig. 4C, $\times 10$ magnification, i.e. 1 pixel corresponding to 0.0423 mm). The drawback related to the inevitable formation of bubbles during the inclusion step was overcome by manually modifying the microscope images (Fig. 4D) before the black&white imaging contrast was further maximized for avoiding shades that could be falsely assigned to PU (Fig. 4E). An example of raw and treated images for a single slice is shown in Figs. 4F.

Taking into account a cross-section of the PU foam roll of 2.54 cm^2 for each of the $N = 17$ slices, the P_r perimeter and the A_r surface of the bridge cross-sections could thus be derived from a home-made Matlab 7.0 soft: $P_r = 31.3$ mm ± 1.4 mm ($CI_{95\%}$) and $A_r = 3.1$ $mm^2 \pm 0.0(2)$ mm^2 ($CI_{95\%}$) for a 1 cm^2 cross-section. Therefore, 1 cm^3 of PU foam resulted in a geometrical surface of $S = 3.1$ $cm^2 \pm 0.1$ cm^2 ($CI_{95\%}$) and a matter volume of $V = 0.031$ $cm^3 \pm 0.0002$ cm^3 ($CI_{95\%}$). This volume corresponded to the volume theoretically occupied by fully-compressed PU foam with no residual open porosity. This yielded to an open porosity of the PU foam of 97%, with a specific (or effective) surface area of about 310 m^{-1}. Hollowing the reactor volume from the lighting tube volume, the 3D reticulated alveolar PU foam developed a surface area of 2850 cm^2 inside the tubular reactor. Considering an available free volume of 1000 cm^3 for the tubular reactor. Taking into account the 572 cm^2 surface area exposed by the surrounding reactor wall, the total surface inside the photoreactor reached 3422 cm^2, the gain in available surface area resulting

from the filling of the reactor by the 3D foam was close to 500%.

3.3. Light transmission measurement

Fig. 5A shows the influence of the cell size and of the foam thickness on the UV-A light transmission (mean sizes of 1900 μm and 4500 μm, and $\geq 4800 \mu m$). The mean light transmission inside the foams was modelled as a function of the distance L from the light source, by a $T_t = e^{-t/\lambda}$ decreasing exponential, with $\lambda_{1900} = 0.35$ cm, $\lambda_{4500} = 0.71$ cm and $\lambda_{>4800} = 1.08$ cm representing the characteristic length for each PU foam. Increasing the mean cell size of the PU foam improved the light transmission within the foam. Indeed, a mean light transmission of about 10% was maintained for a foam thickness of 2.5 cm for a 4800 μm cell size foam, whereas a similar light transmission was obtained for a thickness of 1.5 cm and 0.75 cm through a PU foam with a mean cell size of 4500 μm and 1900 μm, respectively. It could be noted that the deposition of the TiO_2 photocatalyst did not significantly change the light transmission within the foam, with a small decrease in transmittance being observed, as a result of the very large cell size of the high porosity foam (Fig. 5B). An empirical foam thickness of 2.5 cm has thus been chosen for maintaining a light transmission greater than 10% within the reactor, corresponding to a 7 cm width reactor.
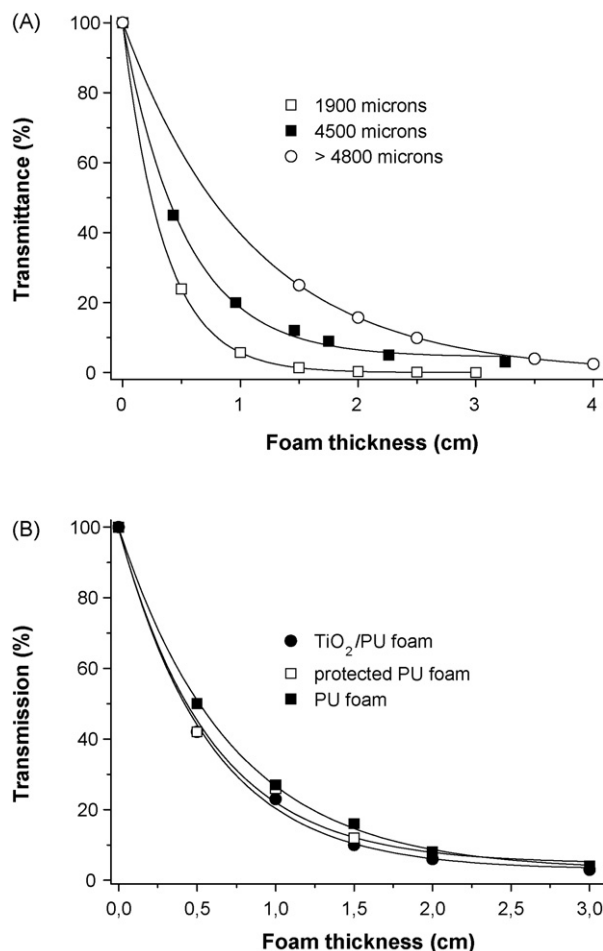

Fig. 5. Transmittance as a function of the foam thickness and of the foam cell size. The curves were fitted using a $T_t = e^{-t/\lambda}$ decreasing exponential model, with λ being the characteristic length. (A) For naked PU foam, and (B) as a function of foam treatment in the case of the 4500 μm cell size PU foam.

3.4. Pressure drop measurement

Targeting the development of a photocatalytic media for environmental applications results from the required necessity of working at low pressure drops notably, in order to remain within a low running cost sustainable chemistry approach. Fig. 6 shows the pressure drop as a function of the inlet gas velocity measured for the 3D-structured reticulated solid PU foam and a commercial silica fiber-based photocatalytic felt.

The photocatalytic foam media could be used at high linear gas velocity, without causing significative pressure drops. It has been derived from a quadratic modelling that working at a linear gas velocity of 16.6 m/s on the solid foam resulted in a pressure drop of 1 bar, whereas this level was reached for a linear gas velocity of 10.7 m/s for the commercial silica fiber-based material. Both materials led to low pressure drops when compared to usual HVAC filters (heating, ventilation and air conditioning filters) incorporated inside ventilation systems and composed of agglomerated 1–40 μm diameter fibers, or to low pressure drop gross G4 prefilters.

Therefore, an alveolar foam reactor could be considered as an intermediate structured reactor, between a filter-like media reactor – exposing a large active surface area but suffering from restrictive pressure drops –, and a tubular reactor – exhibiting a low area of photocatalyst per unit reactor volume but without any pressure drops. In addition, the alveolar solid foam benefits from its large-size alveolar structure for avoiding any plugging of the alveolus.

3.5. Static mixer aspect

In parallel to the strong gain in surface area-to-reactor volume ratio, one of the main interests of using a reticulated alveolar structured foam as photocatalytic support resulted from its static mixer role, which led to a good mixing of the flow inside the reactor and thus to an increase in the surface contact probability. The effect of the three-dimensional reticulated foam on the mixing of the flow (*i.e.* static mixer effect) could be easily evidenced in liquid phase by observing and comparing the flowing of the red amaranth dye, slowly injected through a liquid syringe within a tubular glass reactor, filled or not with the foam media. Although this visualization took place in liquid phase rather in gas phase, it evidenced and evaluated the efficiency of the mixing in laminar regime flowing within structured reactors resulting from the reactor filling by the solid foam. Fig. 7 shows the liquid phase illustration of the static mixer mode of the 3D reticulated PU foam working in two different
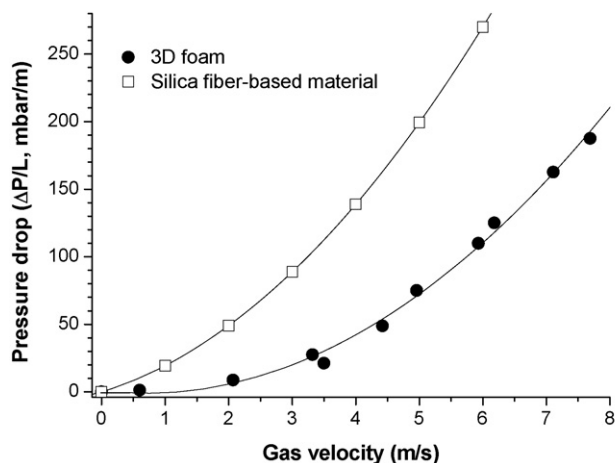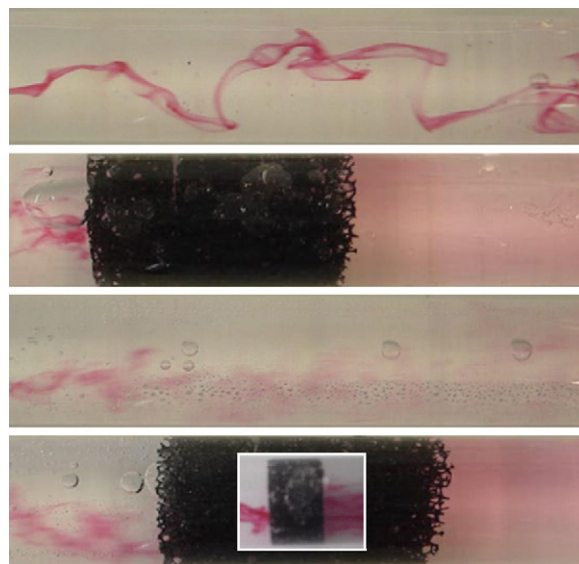

Fig. 7. Illustration of the static mixer mode of the PU foam working in two different laminar flow regimes, using red amaranth dye as probe molecule. Glass reactor diameter of 4 cm and foam length of 6 cm. Inset: illustration with a thin 2 cm thick solid foam.

laminar flow regimes, using red amaranth dye as probe molecule. It was necessary to conduct the experiments in a laminar flow regime so that the static mixer effect of the foam could be evidenced. The figure illustrates the interest of using the structured foam reactor in terms of mixing compared to a tubular reactor, even for a very thin thickness of foam.

Thus, even in the case of flows unpropitious to a good mixing, as a result of a low linear velocity or of a too strong inertia of the airborne microorganisms that could reduce the changes in trajectory (the microorganisms being not considered as mass-free targets like chemicals), the use of a static mixer such as the PU foam would allow an efficient mixture to be obtained within the photocatalytic reactor. Therefore, it would increase the contact probability between the target and the photocatalytic coating.

3.6. Evaluation of the protective coating efficiency

The efficiency of the coating treatment for creating a protective coating has been evaluated by evidencing the diffusion barrier effect of the polysiloxane, by using the ability of the tetrahydrofurane solvent (THF) to dilate the PU foam (Fig. 8A). The delay in expansion of the PU samples with time when plunged into a THF solution evaluated the protection efficiency as a function of the number of protective layers. Fig. 8B and C show the evolution with time immersed in THF, of four PU foam samples after 0–3 protective treatments. The sample expansion was followed by measuring the foam size on photographs, with $T_i(t)$ being the pixel number of a sample coated by i protective films as a function of immersion time, and by comparing the sample sizes through the adimensional parameter $\Theta_i(t)$, with $T_{i,max}$ and $T_{i,min}$, being the maximal and the minimal size of the sample i, respectively,

$$\Theta_i(t) = 100 \times \frac{T_{i,max} - T_i(t)}{T_{i,max} - T_{i,min}}$$

Fig. 8C evidences the efficiency of the diffusion barrier provided by the SIVO coating. Indeed, 50% of the maximal expansion was reached after only 5 min of THF immersion duration for the raw non-protected PU foam, whereas this duration was delayed by more than 30 min with a mono-layer coating, and even reached 60 min for the three-layer protected PU foam. An efficient protec-
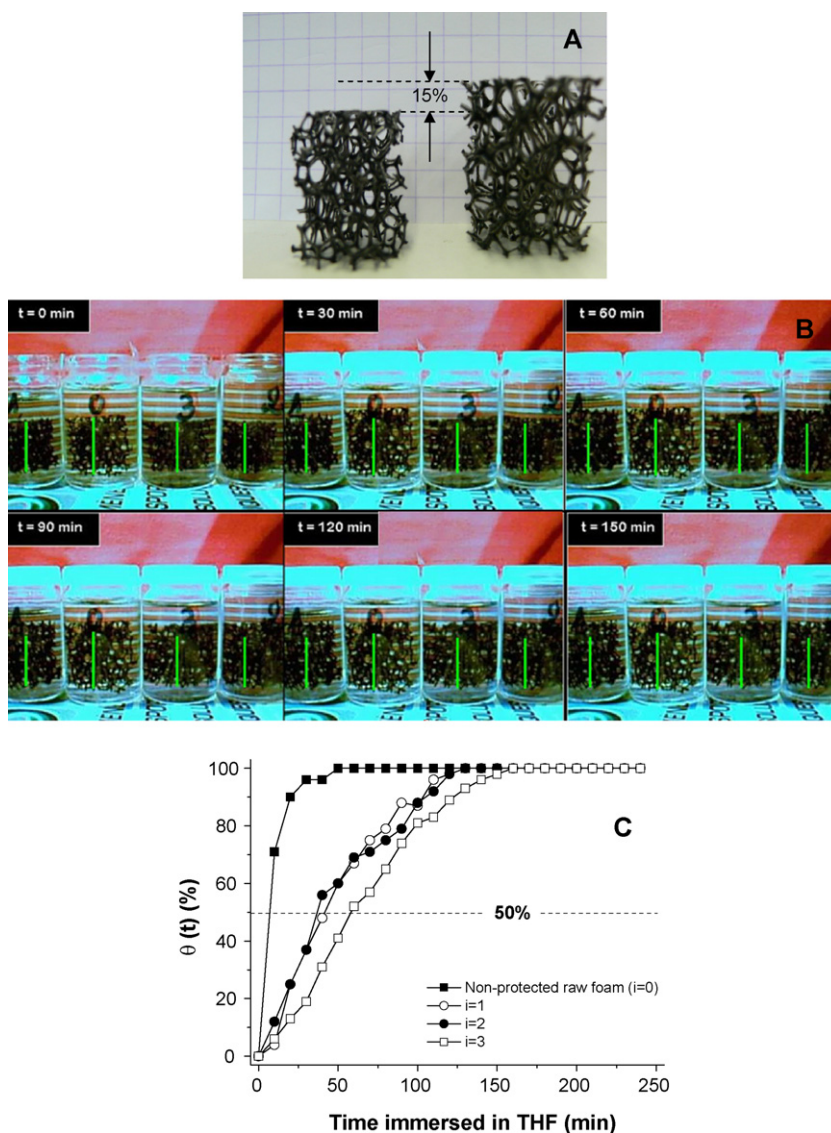

Fig. 6. Pressure drop measurement versus gas velocity for: (●) 3D-structured foam and (□) commercial silica fiber-based photocatalytic felt.

Fig. 8. (A) Non-protected PU foam before and after dilatation by the THF solvent, with a 15% expansion coefficient measured after THF evaporation. (B) Time-evolution of the PU foam immersed in the THF solvent: *from left-to-right*, PU foams coated with 1, 0, 3 and 2 layers. The green line corresponded to the initial height of the samples. (C) Evolution of the dimension-free $\Theta(t)$ parameter as a function of immersion time and of the number of layers formed at the foam surface. (For interpretation of the references to color in this figure legend, the reader is referred to the web version of the article.)

tion of the foam towards chemicals could be already obtained with a mono-layer passivation of the foam, although it could be strongly improved further by forming a multi-layer coating.

Fig. 3A shows the presence of few cracks in the polysiloxane coating for the mono-layer protected foam, probably formed during the polymerization step at 120 °C. This could be attributed to the first expansion of the organic foam support before contracting during the cooling step, creating strains between the PU foam surface and the polysiloxane film strongly bonded to the foam surface, and therefore resulting in the appearance of few cracks. In addition, the THF solvent could consequently slowly diffuse through those irregularities till that the increasing internal strain in the rigid polysiloxane film resulted in its crack, leading to a massive diffusion of the solvent down to the organic polymeric foam. Therefore adding additional protective layers was necessary in order to fully protect the supporting PU foam, by clogging the primary cracks resulting from the formation of the first polysiloxane layer.

The number of polysiloxane layers has been arbitrarily fixed at three, for (i) efficiently protecting the PU surface towards the dif-

fusion of chemical species, and simultaneously, (ii) assuring the mechanical stability of this 3D solid foam media by preventing the organic functions binding the polysiloxane film to the PU surface from a possible photocatalytic oxidation. Recently Paschoalino et al. used polydimethylsiloxane and orthophthalic polyester polymers for preparing flexible TiO$_2$ coatings [36]. TiO$_2$ films were also modified with PDMS by Novotná et al. for preparing photocatalytically active TiO$_2$/PDMS films [37].

4. Air decontamination tests

Table 1 shows the logarithmic reduction in viability and the single-pass survival probability obtained through a TiO$_2$-coated and a foam-filled tubular photoreactor. The experiments were conducted at a total air flow of 5 m^3/h and the tests were performed at a linear flow velocity of 0.36 m/s with a flow residence time of 1.5 s. It has been verified that the *L. pneumophila* bacteria was not very sensitive to the aerosolization process, and therefore could be considered as a valuable microorganism for investigating the decontamination efficiency of the photocatalytic treatment.

In the case of the empty photoreactor working in the seep-flow mode (Fig. 2 *left*), 2 g of TiO$_2$ P25 were coated onto the inner surface of the tube, corresponding to a TiO$_2$ surface density of 3.5 mg/cm^2. By contrast, the increase in available surface area resulting from the use of the three-dimensional foam media, *i.e.* close to 500%, allowed 12 g of TiO$_2$ to be incorporated inside the reactor, corresponding to a rather similar TiO$_2$ surface density of 3.8 mg/cm^2.

The TiO$_2$-free protected PU foam did not show any bactericidal properties, with a LRV of −0.1 and a single-pass survival probability of 118%. Obviously, obtaining a slightly negative LRV value and a survival probability slightly greater that 100% was not surprisingly in the microbiology field. This resulted from the work with biological agents – and airborne biological targets especially –, and from the accuracy of the epifluorescence numeration method. Such value levels corresponded to a zero-decontamination activity. In addition, performing the decontamination test with the 3D-structured foam photocatalyst with powder coating in the absence of any UV-A illumination did not result in any significant decontamination efficiency, with a LRV of 0.1 and a single-pass survival probability of 87%. Thus the decontamination efficiency obtained under UV-A illumination and reported in Table 1 could totally be attributed to the UV-A photocatalysis.

As a reference, the photocatalytic decontamination obtained on the tubular photoreactor working in the seep-flow mode was evaluated, with a LRV of 0.1 and a single-pass survival probability of 79%. This resulted from both the low exposed surface area-to-volume ratio of this photoreactor configuration and the high velocity, pointing out the necessity to fill the reactor volume with a suitable media for targeting working in a traversing-flow mode at high air flow rates.

Such LRV and single-pass survival probability values remained within the measurement error, greatly higher when working with airborne biological agents than when targeting chemical VOC removal, and therefore could be considered as zero- or near zero-decontamination efficiencies.

By contrast, using the 3D-structured foam photocatalyst with aqueous coating led to a logarithmic reduction in viability of 1.0, corresponding to a single-pass survival probability of 10%, even for a short residence time of 1.5 s. Anchoring the TiO$_2$ photocatalyst following the powder-based procedure resulted in slightly better decontamination performances than following the aqueous procedure. Indeed, the powder coating led to a high logarithmic reduction in viability of 1.3 and to a low single-pass survival probability of 6%. The powder procedure resulted in a mean TiO$_2$ surface density of 3.8 mg/cm^2, while a lower mean TiO$_2$ surface density of 1.5 mg/cm^2 was obtained using the aqueous suspension procedure, with less TiO$_2$ being anchored at the substrate surface. In parallel, the SEM images (Fig. 9) showed the roughness of the TiO$_2$ coating obtained following the powder-

Table 1
Logarithmic reduction in viability (LRV) and single-pass survival probability. Total air flow = 5 m^3/h, flow velocity = 0.36 m/s, flow residence time = 1.5 s.

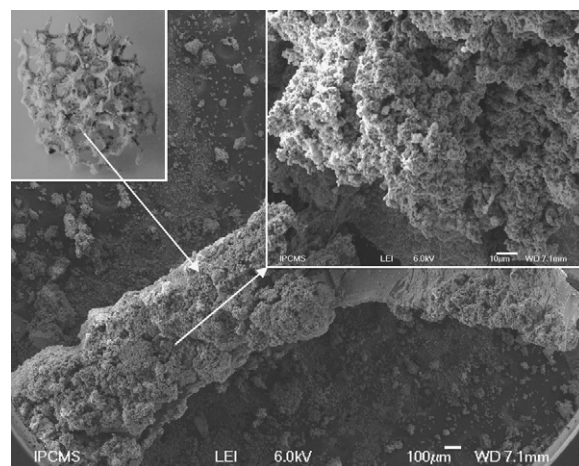| Photoreactors	LRV	Single-pass survival probability
TiO$_2$-coated annular reactor		
Without any UV-A	0.0	91%
With UV-A	0.1	79%
3D-structured foam reactor		
Naked 3D-structured foam with no TiO$_2$ and no UV-A	(−0.1)	(118%)
3D-structured foam with aqueous coating	1.0	10%
3D-structured foam with powder coating		
Without UV-A	0.1	87%
With UV-A	1.31	6%

Fig. 9. SEM images of a foam bridge with powder coating.

based procedure that could be strongly positive for impacting the bacteria onto the coating surface, helped by the anfractuosities developed by the rough surface, and therefore increasing the residence time of the bacteria inside the photoreactor. This highlighted the interest of using the powder-based deposition procedure for designing a foam-based photocatalytic treatment for decontaminating microorganism-containing flowing air. The powder-based procedure displayed the advantage of leading to a chemical binding between the substrate and the photocatalytic grains, with a very stable composite material, whereas by contrast, the aqueous suspension procedure suffered from mechanical stability problems and loss of TiO$_2$ nanoparticle grains due to a bad anchorage, resulting from the hydrophobic nature of the polysiloxane film.

Extrapolating for longer reactors the decontamination efficiency obtained for a length of 26 cm was of interest for approximately estimating the photoreactor length necessary for achieving a given decontamination efficiency. This extrapolation was reported in Fig. 10 for both 3D-structured foam photocatalysts, and compared to the classical TiO$_2$-coated photoreactor. According to the $P(L) = P(1)^L$ relationship derived from the hypothesis of a first order kinetic and a of Plug Flow Reactor, the survival probability $P(L)$ for *L. pneumophila* bacteria as a function of the reactor length L was extrapolated by $P(L) = 0.9824^L$ for the tubular reactor, $P(L) = 0.9152^L$ for the 3D-structured foam photocatalyst with aqueous coating,
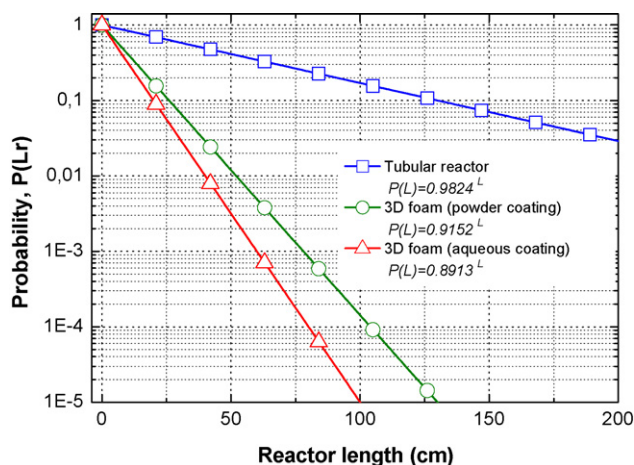

Fig. 10. Extrapolated survival probability $P(L)$ for *L. pneumophila* bacteria as a function of the photoreactor length L, in the case of the tubular reactor and the 3D-structured foam reactor with both powder and aqueous coatings.

and $P(L) = 0.8913^L$ for the 3D-structured foam photocatalyst with powder-based coating.

5. Conclusion

A 3D-structured reticulated polyurethane foam was used as support of a TiO$_2$ particle coating for designing an efficient low pressure drop photocatalytic media allowing tubular reactors to work in a traversing-flow mode rather than in a seep-flow mode. Prior to the TiO$_2$ deposition, the polyurethane foam was protected by an inorganic polysiloxane coating.

The reticulated foam-based media allowed a large increase in the surface area per volume ratio of the reactor to be obtained, together with an improved air-to-surface contact probability ratio induced by the static mixer nature of the foam. The ultra-low pressure drops obtained even at high velocity should allow tubular reactors working in a traversing-flow mode and designing an efficient single-pass decontamination process, targeting *L. pneumophila* bacteria as model tool for airborne microorganisms. The LRV and bacteria survival probability have been chosen as suitable indicators for evaluating the air decontamination efficiency of the photocatalytic treatment when targeting airborne biological agents. Extrapolation as a function of the photoreactor length confirmed the high decontamination efficiency obtained with the 3D-structured foam media. CFD Computational Fluid Dynamics studies are ongoing for taking into account the illumination distribution through the foam.

Acknowledgements

Appendix A. Supplementary data

Supplementary data associated with this article can be found, in the online version, at doi:10.1016/j.jhazmat.2009.10.013.

References

[1] H. De Lasa, B. Serrano, M. Salaices, Novel photocatalytic reactors for water and air treatment, in: H. De Lasa, B. Serrano, M. Salaices (Eds.), Photocatalytic Reaction Engineering, Springer, New York, 2005, pp. 17–47.
[2] O. Alfano, D. Bahnemann, A. Cassano, R. Dillert, R. Goslich, Photocatalysis in water environments using artificial and solar light, Catal. Today 58 (2000) 199–230.
[3] L. Dibble, G. Raupp, Fluidized bed photocatalytic oxidation of trichloroethylene, Environ. Sci. Technol. 26 (3) (1992) 492–495.
[4] D.F. Ollis, Photoreactors for purification and decontamination of air, in: D.F. Ollis, H. Al-Ekabi (Eds.), Photocatalytic Purification and Treatment for Water and Air, Elsevier Sciences Ltd., 1993, pp. 481–494.
[5] N.J. Peill, M.R. Hoffmann, Chemical and physical characterization of a TiO$_2$ coated fiber optic cable reactor, Environ. Sci. Technol. 30 (1996) 2806–2812.
[6] W. Jacoby, D. Blacke, D. Fennell, J. Boulter, L. Vargo, M. George, S. Dolberg, Heterogeneous photocatalysis for the control of volatile organic compounds in indoor air, J. Air Waste Manag. Assoc. 46 (1996) 691–698.
[7] J. Taranto, D. Frochot, P. Pichat, Modeling and optimizing irradiance on planar, folded, and honeycomb shapes to maximize photocatalytic air purification, Catal. Today 122 (2007) 66–77.
[8] G.B. Raupp, A. Alexiadis, Md.M. Hossain, R. Changrani, First-principles modeling, scaling laws and design of structured photocatalytic oxidation reactors for air purification, Catal. Today 69 (2001) 41–49.
[9] Md.M. Hossain, G.B. Raupp, S.O. Hay, T.N. Obee, Three-dimensional developing flow model for photocatalytic monolith reactors, AIChE J. 45 (1999) 1309–1321.
[10] T.N. Obee, R. Brown, TiO$_2$ photocatalysis indoor air applications: effects of humidity, trace contaminant levels on the oxidation rates of formaldehyde, toluene and 1,3-butadiene, Environ. Sci. Technol. 29 (5) (1995) 1223–1231.
[11] M. Singh, I. Salvadó-Estivill, G. Li Puma, Radiation field optimization in photocatalytic monolith reactors for air treatment, AIChE J. 53 (2007) 678–686.
[12] M. Furman, S. Corbel, H. Le Gall, O. Zahraa, M. Bouchy, Influence of the geometry of a monolithic support on the efficiency of photocatalyst for air cleaning, Chem. Eng. Sci. 62 (2007) 5312–5316.
[13] H.F. Lin, K.T. Valsaraj, Development of an optical fiber monolith reactor for photocatalytic wastewater treatment, J. Appl. Electrochem. 35 (2005) 699–708.
[14] P. Du, J.T. Carneiro, J.A. Moulijn, G. Mul, A novel photocatalytic monolith reactor for multiphase heterogeneous photocatalysis, Appl. Catal. A: Gen. 334 (2008) 119–128.
[15] J.T. Richardson, Y. Peng, D. Remue, Properties of ceramic foam catalyst supports: pressure drop, Appl. Catal. Gen. 204 (2000) 19–32.
[16] G. Groppi, E. Tronconi, Design of novel monolith catalyst supports for gas/solid reactions with heat exchange, Chem. Eng. Sci. 55 (12) (2000) 2161–2171.
[17] P. Jain, T. Pradeep, Potential of silver nanoparticle-coated polyurethane foam as an antibacterial water filter, Biotechnol. Bioeng. 90 (1) (2005) 59–63.
[18] A. Yamamoto, H. Imai, Preparation of titania foams having an open cellular structure and their application to photocatalysis, J. Catal. 226 (2004) 462–465.
[19] I.J. Ochuma, O.O. Osibo, R.P. Fishwick, S. Pollington, A. Wagland, J. Wood, J.M. Winterbottom, Three-phase photocatalysis using suspended titania and titania supported on a reticulated foam monolith for water purification, Catal. Today 128 (2007) 100–107.
[20] T. Matsunaga, R. Tomoda, T. Nakajima, H. Wake, Photoelectrochemical sterilization of microbial cells by semiconductor powders, FEMS Microbiol. Lett. 29 (1985) 211–214.
[21] K. Sunada, Y. Kikuchi, K. Hashimoto, A. Fujishima, Bactericidal and detoxification effects of TiO$_2$ thin film photocatalysts, Environ. Sci. Technol. 32 (5) (1998) 726–728.
[22] A.G. Rincon, C. Pulgarin, Bactericidal action of illuminated TiO$_2$ on pure *Escherichia coli* and natural bacterial consortia: post-irradiation events in the dark and assessment of the effective disinfection time, Appl. Catal. B: Environ. 49 (2004) 99–112.
[23] D.M. Blake, P. Maness, Z. Huang, E. Wolfrum, J. Huang, W. Jacoby, Application of the photocatalytic chemistry of titanium dioxide to disinfection and the killing of cancer cells, Sep. Purif. Methods 28 (1) (1999) 1–50.
[24] A. Fujishima, T.N. Rao, D.A. Tryk, Titanium dioxide photocatalysis, J. Photochem. Photobiol., C: Photochem. Rev. 1 (2000) 1–21.
[25] D.Y. Goswami, D.M. Trivedi, S.S. Block, Photocatalytic disinfection of indoor air, J. Sol. Energy Eng. 119 (1997) 92–96.
[26] V. Keller, N. Keller, M.J. Ledoux, M.C. Lett, Biological agent inactivation in a flowing air stream by photocatalysis, Chem. Commun. (2005) 2918–2920.
[27] S. Josset, T. Taranto, N. Keller, V. Keller, M.C. Lett, M.J. Ledoux, V. Bonnet, S. Rougeau, UV-A photocatalytic treatment of high flow rate air contaminated with *Legionella pneumophila*, Catal. Today 129 (1–2) (2007) 215–222.
[28] S.A. Grinshpun, A. Adhikari, T. Honda, K.Y. Kim, M. Toivola, K.S. RamchanderRao, T. Reponen, Control of aerosol contaminants in indoor air: combining the particle concentration reduction with microbial inactivation, Environ. Sci. Technol. 41 (2007) 606–612.
[29] A. Pal, S.O. Pehkonen, L.E. Yu, M.B. Ray, Photocatalytic Inactivation of airborne bacteria in a continuous-flow reactor, Ind. Eng. Chem. Res. 47 (2008) 7580–7585.
[30] M. Lacroix, P. Nguyen, D. Schweich, C. Pham Huu, S. Savin-Poncet, D. Edouard, Pressure drop measurements and modeling on SiC foams, Chem. Eng. Sci. 62 (12) (2007) 3259–3267.
[31] S. Josset, N. Keller, M.-C. Lett, M.J. Ledoux, V. Keller, Numeration methods for targeting photoactive materials in the UV-A photocatalytic removal of microorganisms, Chem. Soc. Rev. 37 (4) (2008) 744–755.
[32] J.G. Fourie, J.P. Du Plessis, Pressure drop modeling in cellular metallic foams, Chem. Eng. Sci. 57 (2002) 2781–2789.
[33] F.C. Buciuman, B. Kraushaar-Czarnetzki, Ceramic foam monoliths as catalyst carriers. 1. Adjustment and description of the morphology, Ind. Eng. Chem. Res. 42 (9) (2003) 1863–1869.
[34] L. Tadrist, M. Miscevic, O. Rahli, F. Topin, About the use of fibrous materials in compact heat exchangers, Exp. Therm. Fluid Sci. 28 (2004) 193–199.
[35] E.A. Moreira, J.R. Coury, The influence of structural parameters on the permeability of ceramic foam, Braz. J. Chem. Eng. 21 (1) (2004) 23–33.
[36] M.P. Paschoalino, J. Kiwi, W.F. Jardim, Gas-phase photocatalytic decontamination using polymer supported TiO$_2$, Appl. Catal. B: Environ. 68 (1–2) (2006) 68–73.
[37] P. Novotná, J. Zita, J. Krýsa, V. Kalousek, J. Rathouský, Two-component transparent TiO$_2$/SiO$_2$ and TiO$_2$/PDMS films as efficient photocatalysts for environmental cleaning, Appl. Catal. B: Environ. 79 (2) (2008) 179–185.